Eigenvalues of the Free Rotation Mode of the Multi-bladed Rotor

Chao Peng(✉) and Alessandro Tasora

Department of Engineering and Architecture,
University of Parma, 43124 Parma, Italy
{chao.peng,alessandro.tasora}@unipr.it

Abstract. The eigenvalues of the free rotation mode of multi-bladed rotor systems are of crucial importance when designing controllers. An unstable free rotation mode of the rotor is unfavorable. In this paper, the Differential Algebraic Equations (DAEs) of the multi-flexible-body system are linearized after having introduced a corotational formulation with respect to the floating frame of reference of the rotating center. The Multi-Blade Coordinate (MBC) transformation is performed to obtain the time-invariant system. The proposed formulations are verified through the numerical experiments carried out on the rotors of increasing complexity: a single rigid body, a rigid rotor, and a flexible rotor. Results reveal that the geometric stiffness matrix and the tangent stiffness matrix of constraints exhibit a centrifugal stiffening effect, moving the eigenvalues toward pure imaginary numbers; in contrast, the inertial stiffness matrix introduces a centrifugal softening effect, pushing the eigenvalues toward real numbers. Generally one has to discard the geometric stiffness matrix, the inertial stiffness matrix, and the tangent stiffness matrix of constraints in the linearized DAEs to obtain the zero eigenvalues for the free rotation mode, whereas the inertial damping matrix can be involved.

Keywords: free rotation mode · multibody linearization · stiffening effect · softening effect

1 Introduction

A multi-bladed rotor system always involves a free *degree of freedom* (DOF) corresponding to the rotation around its axis. For instance, wind turbines and helicopter rotors can rotate freely to exchange kinetic energy between the rotor structure and the surrounding airflow. This rotational DOF introduces the *rigid body mode*, also called *free-free mode*, which is commonly considered to have zero eigenvalues [4]. However, the eigenvalues are unnecessary to be zero; hence we prefer to call it *free rotation mode*.

El-Absy [3] investigated the stability of the rigid body mode of a rotating rotor. Using time-marching simulation, the stability of simple rotors built through three different models with or without the consideration of the effect of the longitudinal displacement due to bending in the inertia and elastic forces

F. Chu and Z. Qin (Eds.): IFToMM 2023, MMS 139, pp. 495–514, 2024.
https://doi.org/10.1007/978-3-031-40455-9_39

are studied. The numerical results demonstrated that the geometric centrifugal stiffening term in the inertia forces is unnecessary to be included to obtain a stable solution. However, only the time series of the beam displacements were plotted to indicate the stability, the eigenvalues were not discussed.

Many researches investigated the stability of multi-bladed rotor systems, however most of them [2,4,5,7,17] focused on the higher order modes, typically the bending modes of the rotor, which are relevant for the design of rotor systems to avoid potential resonances and instabilities. The centrifugal stiffening effect in the rotating beams was realized and its influence on the modal dynamics of rotor systems was well inspected [8,9]. The centrifugal softening effect was also explored [5,20,21].

In the controller design phase, the linearized equations of motion are required to represent the linear controlled systems. The accuracy of the linearization of the original highly nonlinear dynamics system could affect the controller's performance and robustness. Taking the example of a wind turbine, the near-zero frequency bandwidth, which corresponds to the overall rotational characteristics of the rotor system, is the most important range for the controller design to stabilize the rotor speed and maximize the power capture [6]. The transfer functions within the near-zero frequency bandwidth exhibit a direct correlation with the eigenvalues of the free rotation mode in the rotor dynamics system.

In this paper, the analytical linearization of the three-bladed rotor system is derived. The time-invariant system is obtained through *Multi-Blade Coordinate* (MBC) transformation. The eigenvalues of the free rotation mode of rigid and flexible three-bladed rotors are investigated to verify the proposed linearized model. The influences of the geometric stiffness matrix, the inertial stiffness matrix, and the tangent stiffness matrix of constraints on the eigenvalues of the free rotation mode are examined.

2 Methodology

We express the equations for the motion of rigid bodies and finite elements using the Newton-Euler formulation [15]. In this context, we adopt a *mixed basis* approach for the states of rigid bodies and beam nodes: translational DOFs are expressed in the inertial frame whereas, in contrast, rotational DOFs are expressed in the local frame. The coordinates of beam nodes in the mixed basis are denoted as

$$\delta \boldsymbol{q}_m = \left[\delta \boldsymbol{r}_a^T, \boldsymbol{\theta}_l^{\delta T}\right]^T \tag{1}$$

where $\boldsymbol{r}_a$ is the position vector in the inertial frame, $\boldsymbol{\theta}_l^{\delta}$ is the virtual rotation vector in the local frame.

2.1 Corotational Formulation

To simplify the problem, a three-dimensional Euler– Bernoulli beam element is utilized in this study. The material stiffness matrix $\boldsymbol{K}_m$ and the geometric stiffness matrix $\boldsymbol{K}_g$ expressed in the local reference frame of the beam element can

be found in a finite element textbook, such as in [14]. The structural damping matrix generally stabilizes rotor dynamic systems. However, this paper focuses on the linearization and the influences of different terms in the linearized models, so the structural damping matrix is omitted to prevent its impact on the eigenvalues of the free rotation mode of the rotor systems.

A simplified corotational formulation is used to deal with the large deflection of beam elements. A rotation transformation matrix $\boldsymbol{R}_{\diamond} \in \mathbb{R}^{12\times12}$ is introduced [19]:

$$\boldsymbol{R}_{\diamond} = \operatorname{diag}\left[\boldsymbol{R}_{\boldsymbol{F}}, \boldsymbol{R}_{\boldsymbol{A}}^{T}\boldsymbol{R}_{\boldsymbol{F}}, \boldsymbol{R}_{\boldsymbol{F}}, \boldsymbol{R}_{\boldsymbol{B}}^{T}\boldsymbol{R}_{\boldsymbol{F}}\right] \tag{2}$$

where $\boldsymbol{R}_{\boldsymbol{A}}, \boldsymbol{R}_{\boldsymbol{B}} \in \mathbb{R}^{3\times3}$ are the rotation tensors of two nodes A, B of the beam element, $\boldsymbol{R}_{\boldsymbol{F}} \in \mathbb{R}^{3\times3}$ is the rotation tensor of the corotated frame F located in the middle of the centerline.

The tangent stiffness matrix of the Euler– Bernoulli beam element $\boldsymbol{K}_t^0 \in \mathbb{R}^{12\times12}$ is obtained via

$$\boldsymbol{K}_t^0 = \boldsymbol{R}_{\diamond}\left(\boldsymbol{K}_{\boldsymbol{m}} + \boldsymbol{K}_g\right)\boldsymbol{R}_{\diamond}^{T} \tag{3}$$

Transformation to the Floating Frame of Rotation Center. The configuration of the rotating rotor is periodically dependent on time, which can be dealt with by the Lyapunov-Floquet (L-F) transformation. If the rotor is isotropic, MBC transformation is a special case of the L-F transformation [16], can be employed to obtain a time-invariant system. Thanks to its simplicity and computational efficiency, MBC transformation is preferred where possible. Since the mixed basis $\delta\boldsymbol{q}_m$ is chosen, the position vectors of beam nodes at the same spanwise of the blades are not equal; thus, the current formulation does not satisfy the prerequisite of MBC transformation. To address this limitation, the coordinates of blade nodes should be transformed with respect to the rotating center.

The scheme of a three-bladed rotor is shown in Fig. 1. Three auxiliary reference frames H_1, H_2, H_3 are introduced for three blades, respectively, which are rotated by the corresponding azimuth angles $\psi_i, i = 1, 2, 3$ about the rotation axis $\boldsymbol{X}$ from the stationary hub center frame H. The transformation relations are $\boldsymbol{R}_{H_i} = \boldsymbol{R}_H\boldsymbol{R}_{\psi_i}, i = 1, 2, 3$, where $\boldsymbol{R}_H, \boldsymbol{R}_{H_i}$ are the rotation tensors of the reference frames H, H_i, and $\boldsymbol{R}_{\psi_i}$ is the transformation matrix of the rotation about $\boldsymbol{X}$ axis by the azimuth angle ψ_i.

The coordinate of blade nodes $\boldsymbol{q}_m$ can be transformed to the floating reference frame H_i as the variation relation [13]

$$\delta\boldsymbol{q}_m = \boldsymbol{B}_h\delta\boldsymbol{q}_h + \boldsymbol{B}_b\delta\boldsymbol{q}_b \tag{4}$$

where $\boldsymbol{q}_h$ represents the coordinate of the floating reference frame H_i, $\boldsymbol{q}_b$ is the relative coordinate of blade nodes with respect to its corresponding floating reference frame H_i. Moreover, $\boldsymbol{B}_h, \boldsymbol{B}_b \in \mathbb{R}^{6\times6}$ are two auxiliary transformation matrices

$$\boldsymbol{B}_h = \begin{bmatrix} \boldsymbol{I} & -\boldsymbol{R}_{H_i}\widetilde{\boldsymbol{r}_N} \\ \boldsymbol{0} & \boldsymbol{0} \end{bmatrix}, \qquad \boldsymbol{B}_b = \begin{bmatrix} \boldsymbol{R}_{H_i} & \boldsymbol{0} \\ \boldsymbol{0} & \boldsymbol{I} \end{bmatrix} \tag{5}$$

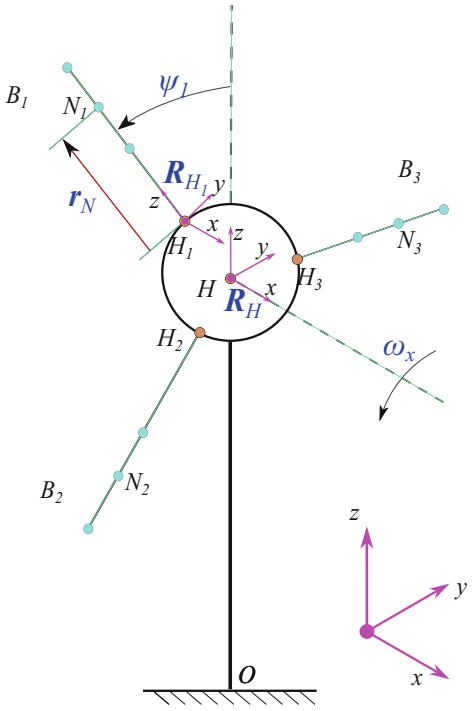

Fig. 1. The scheme of a three-bladed rotor system. The three auxiliary reference frames H_1, H_2, H_3 are located at the same position as H, but shown separately to avoid mess. The three blades are rotated by the corresponding azimuth angles ψ_1, ψ_2, ψ_3. The angles ψ_2, ψ_3 are not shown.

where $\boldsymbol{r}_N$ is the position vector of the blade node N with respect to its corresponding floating reference frame H_i.

Extending the coordinate transformation relation Eq. (4) to two nodes A, B of the beam element, a larger transformation matrix $\boldsymbol{B}_{\text{fc}} \in \mathbb{R}^{12\times 18}$ is introduced

$$\boldsymbol{B}_{\text{fc}} = \begin{bmatrix} \boldsymbol{B}_{\boldsymbol{h}_A} & \boldsymbol{B}_{\boldsymbol{b}_A} & \boldsymbol{0} \\ \boldsymbol{B}_{\boldsymbol{h}_B} & \boldsymbol{0} & \boldsymbol{B}_{\boldsymbol{b}_B} \end{bmatrix} \tag{6}$$

Using the principle of virtual work, the tangent stiffness matrix $\boldsymbol{K}_t^0$ in the original mixed basis $\delta \boldsymbol{q}_m$ can be transformed into the auxiliary mixed basis $\left[\delta \boldsymbol{q}_h^T, \delta \boldsymbol{q}_b^T\right]^T$ as

$$\boldsymbol{K}_t^1 = \boldsymbol{B}_{\text{fc}}^T \boldsymbol{K}_t^0 \boldsymbol{B}_{\text{fc}} \tag{7}$$

where $\boldsymbol{K}_t^1 \in \mathbb{R}^{18\times 18}$, in which the top-left block is the term projected onto the hub center, the bottom-right block is the term of the blade beam element, the off-diagonal blocks are the coupling terms between blade and hub.

The hub block in $\boldsymbol{K}_t^1$ is respect to the floating reference frame H_i which is different for three blades. One needs to rotate $\boldsymbol{K}_t^1$ back to the consistent reference frame H, as

$$\boldsymbol{K}_t^2 = \boldsymbol{R}_{X_i} \boldsymbol{K}_t^1 \boldsymbol{R}_{\boldsymbol{X}_i}^{\boldsymbol{T}} \tag{8}$$

where $\boldsymbol{R}_{X_i} = \text{diag}\left[\boldsymbol{I}_{3\times3}, \boldsymbol{R}_{\psi_i}, \boldsymbol{I}_{12\times12}\right] \in \mathbb{R}^{18\times18}$ is a block diagonal matrix.

The tangent stiffness matrix $\boldsymbol{K}_t^2$ is finally assembled in the system stiffness matrix according to its corresponding coordinate index.

2.2 Constraints

The method of Lagrange multipliers is used to formulate the equations of motion for dynamics systems involving multiple constraints, which represent the joint connections among rigid bodies and beam nodes. The change of the orientation of the reaction forces and torques in joints would generate the geometric stiffness term $\boldsymbol{K}_c = \frac{\partial \boldsymbol{C}_{\boldsymbol{q}}^T}{\partial \boldsymbol{q}} \gamma$ [1], where $\boldsymbol{C}_{\boldsymbol{q}}$ is the Jacobian matrix of the constraint, γ is the Lagrange multipliers which are associated with the reaction forces and torques. The Jacobian matrix $\boldsymbol{C}_{\boldsymbol{q}}$ and the tangent stiffness matrix of holonomic constraints $\boldsymbol{K}_c$ can be evaluated in closed-form analytical expressions in the original mixed basis $\delta \boldsymbol{q}_m$, which have been implemented in the open-source multibody library CHRONO [18]. Similar transformations in Eqs. (7) and (8) are performed for $\boldsymbol{C}_{\boldsymbol{q}}$ and $\boldsymbol{K}_c$ to achieve a consistent basis. These two matrices are used in the DAE of the rotor system.

2.3 Inertial Forces and Torques

In this work, the lumped mass model is assumed for the beam elements. The inertial forces $\boldsymbol{F}_{I_a}$ and the inertial torques $\boldsymbol{M}_{I_l}$, when expressed in the original mixed basis $\delta \boldsymbol{q}_m$, are:

$$\begin{aligned} \boldsymbol{F}_{I_a} &= \nu \ddot{\boldsymbol{r}}_a + \nu \boldsymbol{R} \tilde{\boldsymbol{c}}^T \dot{\boldsymbol{\omega}}_l + \nu \boldsymbol{R} \widetilde{\boldsymbol{\omega}_l} \widetilde{\boldsymbol{\omega}_l} \boldsymbol{c} \\ \boldsymbol{M}_{I_l} &= \nu \tilde{\boldsymbol{c}} \boldsymbol{R}^T \ddot{\boldsymbol{r}}_a + \boldsymbol{J} \dot{\boldsymbol{\omega}}_l + \widetilde{\boldsymbol{\omega}_l} \boldsymbol{J} \boldsymbol{\omega}_l \end{aligned} \tag{9}$$

where ν is the lumped mass at the node, $\boldsymbol{c}$ is the vector of the mass center offset in the local frame of the node, $\boldsymbol{J}$ is the tensor of the moments of inertia in the local frame of the node, $\ddot{\boldsymbol{r}}_a$ is the translational acceleration in the inertial frame, $\boldsymbol{\omega}_l$ is the angular velocity in the local frame, $\boldsymbol{R}$ is the rotation tensor of the local frame of the node.

Using the coordinate transformation in Eq. (4) and its derivatives, after long algebraic manipulations, the inertial forces $\boldsymbol{F}_{I_a}$ and the inertial torques $\boldsymbol{M}_{I_l}$ can be transformed to the auxiliary mixed basis $\left[\delta \boldsymbol{q}_h^T, \delta \boldsymbol{q}_b^T\right]^T$, then linearized through variation techniques, leading to the inertial mass matrix $\boldsymbol{M}_i$, the inertial damping matrix $\boldsymbol{R}_{\boldsymbol{i}}$, and the inertial stiffness matrix $\boldsymbol{K}_i$ [13]. These three inertial matrices are rotated back to the consistent reference frame H with a similar transformation as in Eq. (8), then scattered into the system matrices.

2.4 MBC Transformation

After transforming all the mass, damping, and stiffness matrices to the consistent auxiliary mixed basis $\left[\delta \boldsymbol{q}_h^T, \delta \boldsymbol{q}_b^T\right]^T$, the MBC transformation is performed on both the structural generalized coordinates $\delta \boldsymbol{q}$ and the Lagrange multipliers $\delta \boldsymbol{\gamma}$, leading to the linearized time-invariant DAE [13]:

$$\begin{cases} \boldsymbol{M}_z \delta \ddot{\boldsymbol{z}} + \boldsymbol{R}_z \delta \dot{\boldsymbol{z}} + \boldsymbol{K}_z \delta \boldsymbol{z} + \boldsymbol{C}_{\boldsymbol{q}_z}^T \delta \boldsymbol{\gamma}_z = \boldsymbol{0} & (10) \\ \boldsymbol{C}_{q_\mathrm{T}} \delta \boldsymbol{z} = \boldsymbol{0} & (11) \end{cases}$$

where $\boldsymbol{R}_z$ consists of only the inertial damping matrix $\boldsymbol{R}_i$, which includes the gyroscopic damping term; $\boldsymbol{K}_z$ is composed of the structural material stiffness matrix of beam elements $\boldsymbol{K}_m$, the geometric stiffness matrix of beam elements $\boldsymbol{K}_g$, the inertial stiffness matrix $\boldsymbol{K}_i$, and the tangent stiffness matrix of constraints $\boldsymbol{K}_c$.

2.5 Eigenvalue Analysis

The generalized descriptor form $\boldsymbol{E}_y \delta \dot{\boldsymbol{y}} = \boldsymbol{A}_y \delta \boldsymbol{y}$ of the linearized DAE Eqs. (10) and (11) is built by introducing the state vector $\delta \boldsymbol{y} = \left[\delta \boldsymbol{z}^T \ \delta \dot{\boldsymbol{z}}^T \ \delta \boldsymbol{\gamma}_z^T\right]^T$ and two system matrices

$$\boldsymbol{E}_y = \begin{bmatrix} \boldsymbol{I} & \boldsymbol{0} & \boldsymbol{0} \\ \boldsymbol{0} & \boldsymbol{M}_z & \boldsymbol{0} \\ \boldsymbol{0} & \boldsymbol{0} & \boldsymbol{0} \end{bmatrix}, \qquad \boldsymbol{A}_y = \begin{bmatrix} \boldsymbol{0} & \boldsymbol{I} & \boldsymbol{0} \\ -\boldsymbol{K}_z & -\boldsymbol{R}_z & -\boldsymbol{C}_{\boldsymbol{q}_z}^T \\ -\boldsymbol{C}_{q_\mathrm{T}} & \boldsymbol{0} & \boldsymbol{0} \end{bmatrix} \tag{12}$$

The corresponding eigenvalues can be evaluated using different numerical methods, among these we endorse a recent embodiment of the Krylov-Schur iteration [11] because of its robustness when dealing with clustered and near-zero eigenvalues.

Using this generalized descriptor, one obtains twice the number of eigenvalues as the number of degrees of freedom, plus spurious eigenvalues corresponding to the rows of the constraint jacobian $\boldsymbol{C}_{q_\mathrm{T}}$, if any. For instance, a rigid body freely rotating in 3D space will generate six eigenvalues relative to the three rotations.

The eigenvalues of the free rotation mode always have the smallest magnitude, therefore they can be extracted easily.

3 Numerical Experiments

The proposed approach is verified through a series of numerical experiments on rotors with different complexities.

In all the numerical experiments discussed in these pages, gravity is not considered.

3.1 Single Rigid Body

The first model we investigated is a single rotating rigid body.

The *intermediate axis theorem*, also called as *tennis racket theorem*, deals with a freely rotating rigid body with three distinct principal moments of inertia: the rotation of the rigid body around its minor and major principal axes is stable, while the rotation around its intermediate principal axis is unstable [10]. The intermediate axis theorem provides a reference result for the eigenvalue analysis of a rotor.

For a single rotating rigid body, the mass matrix is

$$\boldsymbol{M} = \text{diag}\,[m, m, m, J_{xx}, J_{yy}, J_{zz}] \tag{13}$$

where m is the mass, J_{xx}, J_{yy}, J_{zz} are the moments of inertia about its three principal axes, respectively. Supposing the rotating center is located at the mass center, the cross term $J_{yz} = 0$.

The damping matrix is

$$\boldsymbol{R} = \begin{bmatrix} \boldsymbol{0} & \boldsymbol{0} \\ \boldsymbol{0} & \widetilde{\boldsymbol{\omega}_l}\boldsymbol{J} - \widetilde{\boldsymbol{J}\boldsymbol{\omega}_l} \end{bmatrix} \tag{14}$$

where $\boldsymbol{J} = \text{diag}\,[J_{xx}, J_{yy}, J_{zz}]$ is the tensor of the moments of inertia, $\boldsymbol{\omega}_l = [\omega_x, \omega_y, \omega_z]^T$ is the angular velocity vector expressed in the local frame of the rigid body.

The stiffness matrix is $\boldsymbol{K} = \boldsymbol{0}$.

The eigenvalues of two cases are investigated: free rotation about three axes, and constrained body with free rotation about the X axis.

Free Rotation About Three Axes. The rigid body rotates about three axes freely. The eigenvalues are listed in Table 1.

In case the three moments of inertia are distinct as $J_{xx} > J_{yy} > J_{zz}$, the eigenvalues for rotation around X (which is the minor principal axis) and Z (which is the major principal axis) are a pair of pure imaginary numbers, implying a constant-amplitude oscillation, whereas the eigenvalues for rotation around Y (which is the intermediate principal axis) are a pair of real numbers, indicating an unstable movement. This result is identical to the intermediate axis theorem.

In case the three moments of inertia hold a relation $J_{xx} = 2J_{yy} = 2J_{zz}$ which mimics an isotropic three-bladed rigid rotor, the eigenvalues for rotation around X (which is the major principal axis, also is the rotation axis of the rigid rotor) are a pair of pure imaginary numbers, and the natural frequency is equal to the angular velocity π. The eigenvalues for rotation around Y and Z axes are zero. There is no unstable mode.

Constrained Body with Free Rotation About the X Axis. The rigid body is allowed to rotate freely about the X axis only. The rotational DOFs about Y and Z axes are constrained by a revolute joint. The eigenvalues are zero, as listed in Table 2.

Table 1. Eigenvalues of a single rigid body in free rotation about three axes. Only two eigenvalues are listed since the other four eigenvalues are zero.

Subcase	m [kg]	J_{xx} [kg m^2]	J_{yy}	J_{zz}	ω_x [rad s^{-1}]	ω_y	ω_z	λ
$J_{xx} > J_{yy} > J_{zz}$	1.3	5.7	3.3	1.9	π	0	0	$\pm 3.79i$
					0	π	0	± 1.75
					0	0	π	$\pm 1.67i$
$J_{xx} = 2J_{yy} = 2J_{zz}$	1.3	5.7	2.85	2.85	π	0	0	$\pm \pi i$
					0	π	0	$0, 0$
					0	0	π	$0, 0$

Table 2. Eigenvalues of a single rigid body in free rotation about X axis.

Subcase	m [kg]	J_{xx} [kg m^2]	J_{yy}	J_{zz}	ω_x [rad s^{-1}]	ω_y	ω_z	λ
$J_{xx} > J_{yy} > J_{zz}$	1.3	5.7	3.3	1.9	π	0	0	$0, 0$
$J_{xx} = 2J_{yy} = 2J_{zz}$	1.3	5.7	2.85	2.85	π	0	0	$0, 0$

3.2 Rigid Rotor

An ideal isotropic rigid rotor is investigated as the second model. As shown in Fig. 2, the rigid rotor consists of four rigid bodies: the hub H located at the rotating center, and three bearings P_1, P_2, P_3 located at the same radius but equally distributed azimuth positions. The three bearings are linked to the hub by three fixed joints C_1, C_2, C_3, respectively. The hub is linked to the ground by the joint C_R, of which the rotational DOFs can be adjusted to free the rotation about three axes or only the X axis.

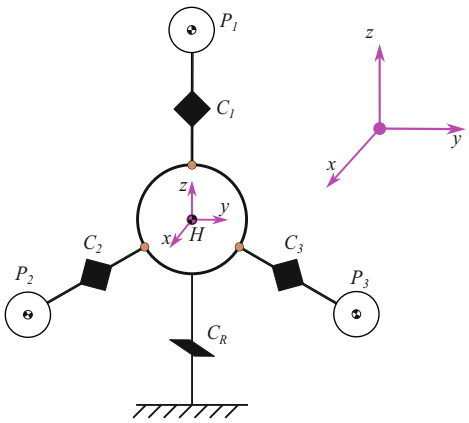

Fig. 2. The scheme of the three-bladed rigid rotor.

The moments of inertia of the hub and bearings are set as zero to facilitate the comparison with the single rigid body model. The masses of the hub and the bearing are 629 kg and 2222 kg, respectively. The radii between the hub and bearings are 0.2 m.

Since the rigid rotor has no flexible finite element, the material stiffness matrix $\boldsymbol{K_m}$ and the geometric stiffness matrix $\boldsymbol{K}_g$ are absent. The influence of the inertial stiffness matrix $\boldsymbol{K}_i$, the inertial damping matrix $\boldsymbol{R_i}$, and the tangent stiffness matrix of constraints $\boldsymbol{K}_c$ on the eigenvalues are investigated through including or excluding them in Eq. (10).

Similarly, two cases with different rotational constraints are investigated.

Table 3. Eigenvalues of a three-bladed rigid rotor. The "×" symbol means the corresponding matrix is included. For the case of free rotation about three axes, the other four eigenvalues are zero, thus not listed.

Subcase	$\boldsymbol{K}_i$	$\boldsymbol{R_i}$	$\boldsymbol{K}_c$	ω_x	λ
Free rotation about three axes		×		0	$0, 0$
				π	$\pm\pi i$
	×	×	×	0	$0, 0$
				π	$\pm\pi i$
Free rotation about X axis		×		0	$0, 0$
				π	$0, 0$
		×	×	0	$0, 0$
				π	$\pm\pi i$
	×	×		0	$0, 0$
				π	$\pm\pi$
	×	×	×	0	$0, 0$
				π	$0, 0$

Since the ideal rigid rotor can be lumped to a single rigid body with the relation $J_{xx} = 2J_{yy} = 2J_{zz}$, its eigenvalues should be identical with the results in Tables 1 and 2.

As shown in Table 3, if the rotational velocity around the rotation axis X is zero, the centrifugal forces and gyroscopic torques are zero, thus the matrices $\boldsymbol{K}_i, \boldsymbol{R_i}, \boldsymbol{K}_c = \boldsymbol{0}$, leading to zero eigenvalues for the two different constraint conditions.

When the rotational velocity is π, in case of free rotation about three axes, if the inertial damping matrix $\boldsymbol{R_i}$ is included, the eigenvalues are $\pm\pi i$, thus the natural frequency is equal to the rotational velocity, which is identical with the result in Table 1. In this case, the matrices $\boldsymbol{K}_i, \boldsymbol{K}_c$ must be absent or present at the same time, otherwise the eigenvalues deviate from $\pm\pi i$, leading to erroneous results which are not listed in Table 3 for the sake of conciseness.

When the rotational velocity is π, in case of free rotation about X axis, if $\boldsymbol{R_i}$ is included and if $\boldsymbol{K}_i, \boldsymbol{K}_c$ are absent or present at the same time, the eigenvalues are zero, which is identical with the result in Table 2. If only $\boldsymbol{K}_c$ is involved on the basis of $\boldsymbol{R_i}$, the eigenvalues change to $\pm\pi i$; if only $\boldsymbol{K}_i$ is involved on the basis of $\boldsymbol{R_i}$, the eigenvalues change to $\pm\pi$.

The tangent stiffness matrix of constraints $\boldsymbol{K}_c$ moves the eigenvalues away from zero along the imaginary axis, implying a stiffening effect; in contrast, the inertial stiffness matrix $\boldsymbol{K}_i$ moves the eigenvalues away from zero along the real axis, implying a softening effect. For the rigid rotor, the stiffening effect of $\boldsymbol{K}_c$ and the softening effect of $\boldsymbol{K}_i$ can counteract completely.

The identical results between Table 3 and Table 1, 2 indicate that the linearized DAEs established using the proposed corotational formulation with respect to the floating frame of reference of the rotating center and the MBC transformation are applicable on the eigenvalue analysis of three-bladed rotors.

3.3 Flexible Rotor

Three flexible blades are linked to the three bearings of the rigid rotor model via fixed joints to make the system closer to the wind turbine rotor. The blades are straight with constant rectangle cross section in 0.6 m×0.2 m. The blade length is 6.0 m. The blade material is assumed as steel with elastic modulus $E = 2.1 \times 10^{11}$Pa, Poisson's ratio $\mu = 0.3$, and density $\rho = 7800$ kg m^{-3}.

The scheme of the flexible rotor is shown in Fig. 3.

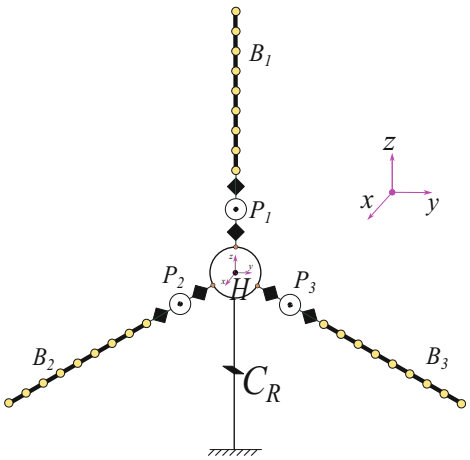

Fig. 3. The scheme of the three-bladed flexible rotor.

Every blade is discretized to 10 Euler– Bernoulli beam elements. The eigenvalues of the flexible rotor are solved using the proposed method. Only the eigenvalues of the free rotation mode of the rotor are listed in this study.

No External Forces. When no external forces act on the blades, the eigenvalues of the two different constraint conditions are reported in Table 4.

Table 4. Eigenvalues of a three-bladed flexible rotor without external forces. The "×" symbol means the corresponding matrix is included. The material stiffness matrix $\boldsymbol{K_m}$ is included in all cases.

Subcase	$\boldsymbol{K}_g$	$\boldsymbol{K}_i$	$\boldsymbol{R_i}$	$\boldsymbol{K}_c$	ω_x	λ		
Free rotation about three axes			×		0	$0, 0$	$0, 0$	$0, 0$
					π	$\pm\pi i$	± 0.0063	$\pm 0.0139i$
	×	×	×	×	0	$0, 0$	$0, 0$	$0, 0$
					π	$\pm\pi i$	± 0.0108	$\pm 0.0141i$
Free rotation about X axis			×		0	$0, 0$		
					π	± 0.0081		
	×		×		0	$0, 0$		
					π	$\pm 3.0598i$		
		×	×		0	$0, 0$		
					π	± 3.1380		
			×	×	0	$0, 0$		
					π	$\pm 0.6964i$		
	×	×	×	×	0	$0, 0$		
					π	$\pm 0.0072i$		

When the rotational velocity is π, in case of free rotation about three axes, the eigenvalues $\pm\pi i$ appear as expected, but the other four eigenvalues deviate to two pairs of real numbers and pure imaginary numbers with small magnitudes, which tend to be due to numerical errors.

When the rotational velocity is π, in case of free rotation about X axis, if only $\boldsymbol{R_i}$ is included, the eigenvalues change to a pair of small real numbers ± 0.0081; in contrast, if the four matrices $\boldsymbol{K}_g, \boldsymbol{K}_i, \boldsymbol{R_i}, \boldsymbol{K}_c$ are all included, the eigenvalues change to a pair of small pure imaginary numbers $\pm 0.0072i$. This result is considered to be due to numerical errors.

If $\boldsymbol{K}_g$ or $\boldsymbol{K}_c$ are involved based on $\boldsymbol{R_i}$ individually, the eigenvalues change to a pair of imaginary numbers, which implies that $\boldsymbol{K}_g$ and $\boldsymbol{K}_c$ contribute a stiffening effect; in contrast, if $\boldsymbol{K}_i$ is involved based on $\boldsymbol{R_i}$, the eigenvalues become to a pair of real numbers, which implies that $\boldsymbol{K}_i$ contributes a softening effect. For the flexible rotor without external forces, the stiffening effect of $\boldsymbol{K}_g, \boldsymbol{K}_c$ and the softening effect of $\boldsymbol{K}_i$ can counteract completely.

With External Forces. The out-of-plane forces $\boldsymbol{F}_x = 725630.0\ N$ and the inplane forces $\boldsymbol{F}_y = 439010.0\ N$ are equally distributed at blade nodes to mimic

the aerodynamic loadings on the rotor. The forces follow the orientation of blade nodes when the rotor deflects, which are called *follower forces*.

The hub is locked firstly in the quasi-static equilibrium analysis, then the rotational DOF about X axis is freed to perform the eigenvalue analysis.

Since the wind turbine rotor has only one rigid motion DOF: the rotation about X axis, the case of free rotation about three axes is not discussed here.

The out-of-plane and inplane deflections of the blade tip in case of rotational velocity 0 rad s^{-1} are 0.24 m and 0.016 m, respectively. The ratio of deflections to the blade length is less than 5 %, thus it is still in the range of small deflections.

The eigenvalues of the free rotation mode of the flexible rotor with external follower forces are listed in Table 5.

Table 5. Eigenvalues of a three-bladed flexible rotor with external follower forces. The "×" symbol means the corresponding matrix is included. The material stiffness matrix $\boldsymbol{K_m}$ is included in all cases.

Subcase	$\boldsymbol{K}_g$	$\boldsymbol{K}_i$	$\boldsymbol{R}_i$	$\boldsymbol{K}_c$	ω_x	λ
Free rotation about X axis			×		0	$0, -0.0002$
					π	± 0.0002
	×		×		0	± 0.7034
					π	$\pm 2.9768i$
		×	×		0	± 0.0001
					π	± 3.1379
			×	×	0	± 0.2800
					π	$\pm 0.6388i$
	×	×	×	×	0	± 0.7570
					π	± 0.7598

If only $\boldsymbol{R_i}$ is included, the eigenvalues are near zero. The deviation away from zero is due to numerical errors.

If $\boldsymbol{K}_g$ is involved based on $\boldsymbol{R_i}$, in case of $\omega_x = 0$, the eigenvalues change from near zero to a pair of real numbers ± 0.7034, which implies that the geometric stiffness term due to transverse external follower forces $\boldsymbol{F}_x, \boldsymbol{F}_y$ has a softening effect; in case of $\omega_x = \pi$, the eigenvalues change to a pair of pure imaginary numbers $\pm 2.9768i$. The increase of the rotational velocity moves the eigenvalues from the real axis to the imaginary axis, which implies that the geometric stiffness term due to the centrifugal forces has a stiffening effect.

If $\boldsymbol{K}_i$ is involved based on $\boldsymbol{R_i}$, in case of $\omega_x = 0$, the eigenvalues are still near zero, that is because the quadratic velocity terms of the inertial forces are zero, leading to $\boldsymbol{K}_i = \boldsymbol{0}$; in case of $\omega_x = \pi$, the eigenvalues change to a pair of real numbers ± 3.1379, which confirms the softening effect of $\boldsymbol{K}_i$.

If $\boldsymbol{K}_c$ is involved based on $\boldsymbol{R_i}$, in case of $\omega_x = 0$, the eigenvalues change from near zero to a pair of real numbers ± 0.2800, which implies that the tangent

stiffness term of constraints due to transverse external follower forces $\boldsymbol{F}_x, \boldsymbol{F}_y$ has a softening effect; in case of $\omega_x = \pi$, the eigenvalues change to a pair of pure imaginary numbers $\pm 0.6388i$. The increase of the rotational velocity moves the eigenvalues from the real axis to the imaginary axis, which confirms that the tangent stiffness term of constraints due to the centrifugal forces has a stiffening effect.

If the four matrices $\boldsymbol{K}_g, \boldsymbol{K}_i, \boldsymbol{R}_i, \boldsymbol{K}_c$ are all included, the eigenvalues change from near zero to a pair of real numbers, which means the rotor cannot rotate stably.

The eigenvalues of the free rotation mode of the rotor, which are the poles of the system matrix in the state-space representation of the linearized dynamics system, should be zero or at least near zero, otherwise it is impractical to design the controller. In view of a proper controller design, one has to discard the geometric stiffness matrix $\boldsymbol{K}_g$, the inertial stiffness matrix $\boldsymbol{K}_i$, and the tangent stiffness matrix of constraints $\boldsymbol{K}_c$, whereas the inertial damping matrix $\boldsymbol{R_i}$ can be included.

Interpretation of the Stiffening and Softening Effects. The stiffening and softening effects of the geometric stiffness matrix $\boldsymbol{K}_g$, the tangent stiffness matrix of constraints $\boldsymbol{K}_c$, and the inertial stiffness matrix $\boldsymbol{K}_i$ are interpreted, respectively.

Geometric Stiffness Matrix. The geometric stiffness matrix $\boldsymbol{K}_g$ derived based on the linear assumption of the finite beam element [14], is proportional to the internal axial forces of the beam elements. If the internal axial forces tend to stretch the beams, like the guitar string, $\boldsymbol{K}_g$ exhibits the stiffening effect to increase the natural frequencies. In contrast, if the internal axial forces tend to compress the beams, like the cabled tower of a wind turbine, $\boldsymbol{K}_g$ contributes the softening effect to decrease the natural frequencies, leading to the buckling instability in extreme cases.

If the transverse external forces follow the orientation of the nodes when the beam is deflected, which are follower forces, as shown in Fig. 4a, the force $\boldsymbol{F}_j$ acting on the node N_j results in an axial compression force $\boldsymbol{F}_p = \boldsymbol{F}_j \sin(\theta_j - \theta_i)$ within the inner node N_i. In this case, the geometric stiffness matrix $\boldsymbol{K}_g$ contributes the softening effect.

If the transverse external forces maintain a consistent direction relative to the inertial frame, irrespective of the beam deflection, which are called *constant-directional forces* in this paper, as shown in Fig. 4b, the force $\boldsymbol{F}_j$ acting on the node N_j results in an axial stretching force $\boldsymbol{F}_p = \boldsymbol{F}_j \sin(\theta_j)$. In this case, the geometric stiffness matrix $\boldsymbol{K}_g$ exhibits the stiffening effect. Another numerical experiment is conducted for the flexible rotor with external constant-directional forces, in which only the out-of-plane forces $\boldsymbol{F}_x = 725630.0\ N$ are applied and the inplane forces $\boldsymbol{F}_y = \boldsymbol{0}$ to reserve the isotropy of the rotor. As listed in Table 6, the eigenvalues move from zero to pure imaginary numbers after involving $\boldsymbol{K}_g$, thus the stiffening effect is confirmed.

Since the centrifugal forces always tend to stretch the blades, the geometric stiffness matrix $\boldsymbol{K}_g$ from the centrifugal forces generates the stiffening effect for the rotating blades.

Tangent Stiffness Matrix of Constraints. The tangent stiffness matrix of constraints $\boldsymbol{K}_c$ arises from the change of the orientation of the reaction forces and torques in the joints. Minaker [12] derived the closed-form expressions for several joints, and revealed its impact on the eigenvalues of the vehicle suspension systems. $\boldsymbol{K}_c$ is proportional to the reaction forces and torques. A simple example to demonstrate the effects of $\boldsymbol{K}_c$ is the pendulum. If $\boldsymbol{K}_c$ is neglected, the eigenvalues of the pendulum under gravity are two zeros which are incorrect.

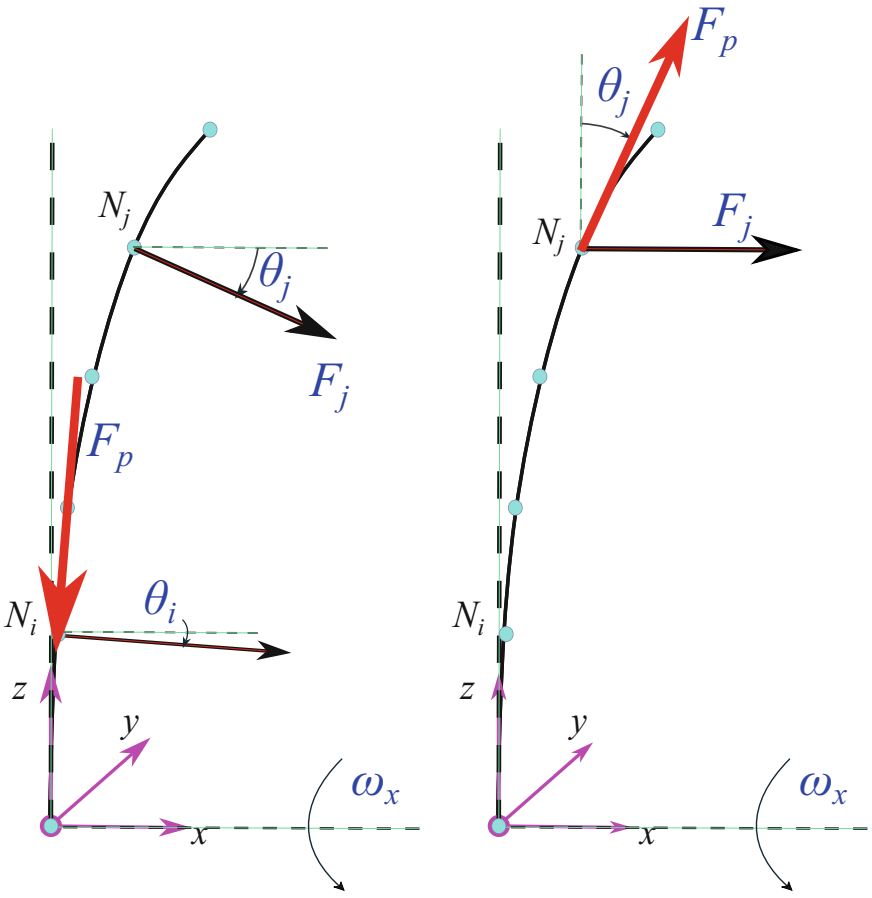

(a) *Follower forces.* (b) *Constant-directional forces.*

Fig. 4. Two distinct external forces exert different effects on the deflected beam.

Table 6. Eigenvalues of a three-bladed flexible rotor with external constant-directional forces. The "×" symbol means the corresponding matrix is included. The material stiffness matrix $\boldsymbol{K_m}$ is included in all cases.

Subcase	$\boldsymbol{K}_g$	$\boldsymbol{K}_i$	$\boldsymbol{R_i}$	$\boldsymbol{K}_c$	ω_x	λ
Free rotation about X axis			×		0	$0, 0.0001$
					π	± 0.0001
	×		×		0	$\pm 0.9740i$
					π	$\pm 3.2068i$

For a normal pendulum shown in Fig. 5a, gravity generates a pulling force $\boldsymbol{F}_c$ at the root joint, which is similar to the axial stretching force in the beam. In this case, the tangent stiffness matrix of constraints $\boldsymbol{K}_c$ provides the stiffening effect, moving the eigenvalues from zero to $\pm\sqrt{g/L}i$.
For an inverted pendulum shown in Fig. 5b, gravity generates a pushing force $\boldsymbol{F}_c$ at the root joint, which is similar to the axial compression force in the beam. In this case, the tangent stiffness matrix of constraints $\boldsymbol{K}_c$ provides the softening effect, changing the eigenvalues from zero to $\pm\sqrt{g/L}$ which implies an unstable motion.
When the transverse external follower forces are applied, similar to the axial compression force $\boldsymbol{F}_p$ shown in Fig. 4a, a pushing force $\boldsymbol{F}_c$ will be generated at the root joint. Analogy to the inverted pendulum, the tangent stiffness matrix of constraints $\boldsymbol{K}_c$ provides the softening effect.

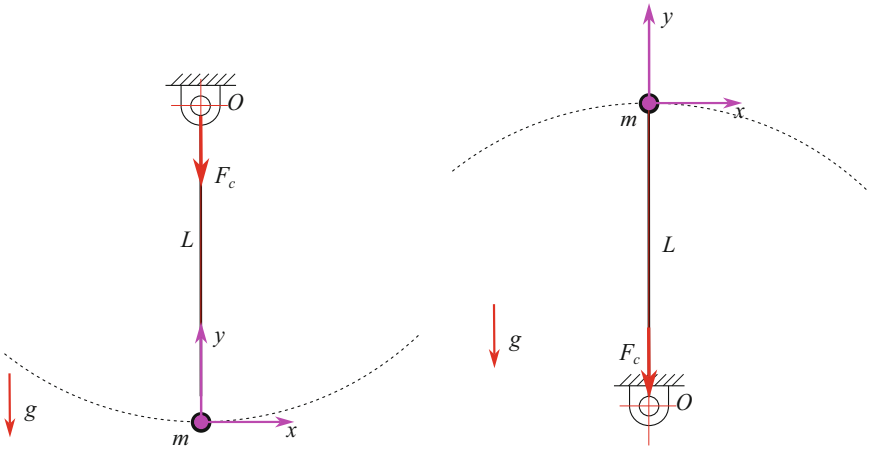

(a) *Normal pendulum.* (b) *Inverted pendulum.*

Fig. 5. Two pendulum models. g is the gravity acceleration, L is the pendulum length.

The centrifugal forces always generate a pulling force $\boldsymbol{F}_c$ at the root joint. Analogy to the normal pendulum, the tangent stiffness matrix of constraints $\boldsymbol{K}_c$ provides the stiffening effect.

Inertial Stiffness Matrix. The inertial stiffness matrix $\boldsymbol{K}_i$ involves an important term $\boldsymbol{k}_{22} = -\widetilde{\boldsymbol{r}_N}\widetilde{\boldsymbol{f}_c}$ in the hub block of the detailed expression [13], where $\boldsymbol{f}_c = \nu\widetilde{\boldsymbol{\omega}_{l_H}}\widetilde{\boldsymbol{\omega}_{l_H}}\boldsymbol{r}_N$ is the centrifugal forces of the nodes of the rotating beams. ν is the lumped mass at the node, and $\boldsymbol{\omega}_{l_H}$ is the angular velocity of the rotating center H in the local frame. Since the centrifugal forces consistently point towards the tip of the rotating beams, and because of the presence of the minus sign in $\boldsymbol{k}_{22}$, negative stiffness values accumulate at the hub block of the system stiffness matrix. Ultimately, the inertial stiffness matrix $\boldsymbol{K}_i$ consistently contributes a softening effect.

The stiffening and softening effects of $\boldsymbol{K}_g, \boldsymbol{K}_c, \boldsymbol{K}_i$ are summarized in Table 7.

Table 7. The stiffening and softening effects of the geometric stiffness matrix $\boldsymbol{K}_g$, the tangent stiffness matrix of constraints $\boldsymbol{K}_c$, and the inertial stiffness matrix $\boldsymbol{K}_i$ from several different forces.

Matrix	Force	Effect
Geometric stiffness matrix $\boldsymbol{K}_g$	Transverse external follower forces	Softening
	Transverse external constant-directional forces	Stiffening
	Centrifugal forces	Stiffening
Tangent stiffness matrix of constraints $\boldsymbol{K}_c$	Transverse external follower forces	Softening
	Centrifugal forces	Stiffening
Inertial stiffness matrix $\boldsymbol{K}_i$	Centrifugal forces	Softening

Parameter Sweeping Analysis. The parameter sweeping analysis is performed to investigate the relationship of the eigenvalues of the free rotation mode with respect to the rotor rotational speed and external forces.

Only the case of free rotation about X axis is studied. The four matrices $\boldsymbol{K}_g, \boldsymbol{K}_i, \boldsymbol{R_i}, \boldsymbol{K}_c$ are all included in the parameter sweeping analysis.

Rotational Speed. The constant external follower forces $\boldsymbol{F}_x$= 725 630.0 N, $\boldsymbol{F}_y$= 439 010.0 N are applied on blade nodes. The rotor rotational speed is swept from 0 to 600 r min^{-1}. As shown in Fig. 6, when the rotor speed increases, the eigenvalues move from a pair of real numbers toward zero and reach zero at approx. 290 r min^{-1}, then deviate away from zero to a pair of pure imaginary numbers. The stiffening effect of $\boldsymbol{K}_g, \boldsymbol{K}_c$ due to the centrifugal forces and the softening effect of $\boldsymbol{K}_i$ compete with each other. In the low rotational speed

range, the softening effect of $\boldsymbol{K}_i$ dominates, leading to real eigenvalues. In the high rotational speed range, the stiffening effect of $\boldsymbol{K}_g, \boldsymbol{K}_c$ dominates, leading to imaginary eigenvalues. At a certain rotational speed, zero eigenvalues are obtained when they are canceled out.

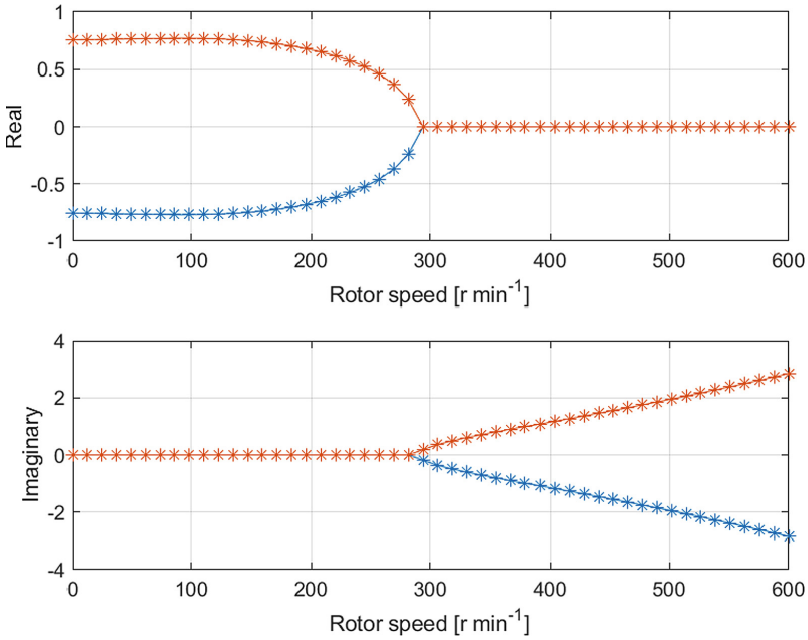

Fig. 6. Eigenvalues of the free rotation mode of the rotor with respect to the rotor rotational speed.

External Forces. The rotor rotational speed is set as πrad s^{-1}. The external follower forces distributed on the blade nodes are swept from 0 to $\boldsymbol{F}_x$= 725 630.0 N, $\boldsymbol{F}_y$= 439 010.0 N. As depicted in Fig. 7, when the external follower forces increase, the eigenvalues disperse away from zero along the real axis proportionally to the force amplitude, which is because the softening effect of $\boldsymbol{K}_g$ induced by transverse external follower forces grows correspondingly. The eigenvalues at zero forces are $\pm 0.0072i$, which is due to numerical errors as explained in Table 4.

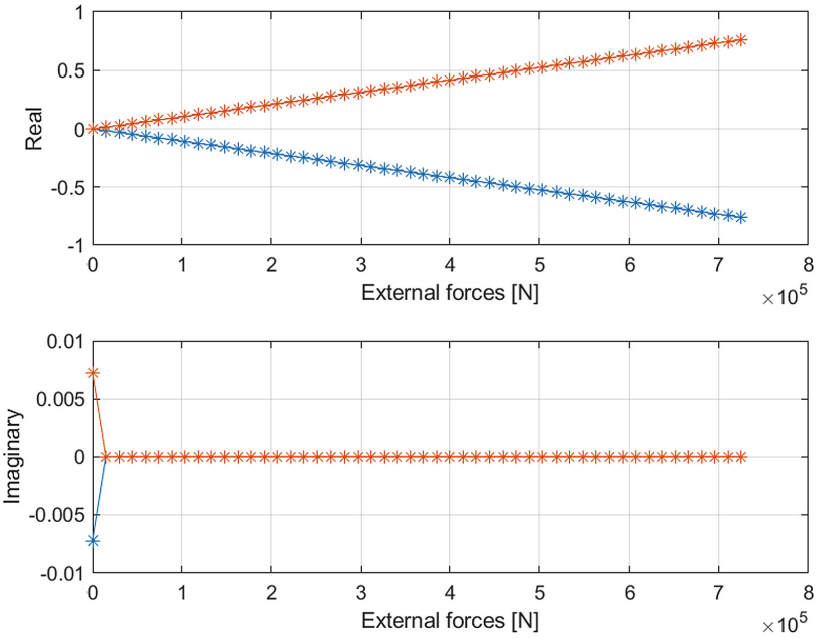

Fig. 7. Eigenvalues of the free rotation mode of the rotor with respect to the external follower forces applied on the blade nodes.

4 Conclusions

Eigenvalues of the free rotation mode of three-bladed rotor systems are investigated. A corotational formulation with respect to the floating frame of reference of the rotating center is applied to the rotor dynamics system. An analytical linearization of the constrained multi-flexible-body DAE is performed, including the geometrical stiffness matrix due to internal forces $\boldsymbol{K}_g$, the inertial stiffness matrix $\boldsymbol{K}_i$, the inertial damping matrix $\boldsymbol{R_i}$ and the tangent stiffness matrix of constraints $\boldsymbol{K}_c$. The MBC transformation is implemented to obtain the time-invariant system, followed by the eigenvalue analysis. Different numerical experiments are carried out on rotors of increasing complexity: a single rigid body, a rigid rotor, and a flexible rotor. It is demonstrated that the linearized DAE formulated using the proposed approach is applicable to the eigenvalue analysis of three-bladed rotors. We discussed the influence of the four matrices $\boldsymbol{K}_g, \boldsymbol{K}_i, \boldsymbol{R}_i, \boldsymbol{K}_c$ on the eigenvalues of the free rotation mode of the rotor. The terms in the geometrical stiffness matrix $\boldsymbol{K}_g$ due to transverse external follower forces, the tangent stiffness matrix of constraints $\boldsymbol{K}_c$ due to transverse external follower forces and the inertial stiffness matrix $\boldsymbol{K}_i$ due to centrifugal forces exhibit a softening effect, moving the eigenvalues toward real numbers. The terms of the geometrical stiffness matrix $\boldsymbol{K}_g$ due to centrifugal forces, the tangent stiffness matrix of constraints $\boldsymbol{K}_c$ due to centrifugal forces, introduce

a stiffening effect that pushes the eigenvalues toward pure imaginary numbers. Aiming at a proper controller design, in order to obtain the zero eigenvalues of the free rotation mode, generally one has to discard the geometric stiffness matrix $\boldsymbol{K}_g$, the inertial stiffness matrix $\boldsymbol{K}_i$, and the tangent stiffness matrix of constraints $\boldsymbol{K}_c$ in the linearized DAE, whereas, the inertial damping matrix $\boldsymbol{R_i}$ can be used anyway. The parameter sweeping analysis demonstrates that the zero eigenvalues could be probably reached at a certain rotational speed even if the four matrices $\boldsymbol{K}_g, \boldsymbol{K}_i, \boldsymbol{R_i}, \boldsymbol{K}_c$ are all considered. The blade external follower forces tend to move the eigenvalues toward real numbers, and thus are unfavorable for the stability of the free rotation mode of the rotor.

Further research should consider a rigorous corotational formulation for the beam finite elements, as well as a new finite element based on the Geometrically Exact Beam (GEB) theory. It is interesting to find the conditions of zero eigenvalues when all the geometric nonlinear terms $\boldsymbol{K}_g, \boldsymbol{K}_i, \boldsymbol{K}_c$ are considered.

References

1. Bauchau, O.A.: Flexible Multibody Dynamics. Springer, Solid mechanics and its applications (2010). https://doi.org/10.1007/978-94-007-0335-3
2. Berzeri, M., Shabana, A.A.: Study of the centrifugal stiffening effect using the finite element absolute nodal coordinate formulation. Multibody Sys.Dyn. **7**, 357–387 (2002)
3. El-Absy, H., Shabana, A.A.: Geometric stiffness and stability of rigid body modes. J. Sound Vib. **207**(4), 465–496 (1997)
4. Genta, G.: Dynamics of Rotating Systems. Mechanical Engineering Series. Springer, New York (2007). https://doi.org/10.1007/0-387-28687-X
5. Genta, G., Silvagni, M.: On centrifugal softening in finite element method Rotordynamics. J. Appl. Mech. **81**(1), 011001 (2013)
6. Roig, M.G.: Application of model predictive control to wind turbines (2017)
7. Hansen, M.: Stability analysis of three-bladed turbines using an eigenvalue approach. In: 42nd AIAA Aerospace Sciences Meeting and Exhibit (2004)
8. Lokanna, H., Gupta, S.S., Sucheendran, M.M.: Modeling of geometrical stiffening in a rotating blade-a review. J. Sound Vibr. **548**, 117526 (2023)
9. Huang, J., Wang, K., Tang, J., Xu, J., Hanwen, S.: An experimental study of the centrifugal hardening effect on rotating cantilever beams. Mech. Syst. Sig. Process. **165**, 108291 (2022)
10. Leine, R., Capobianco, G., Bartelt, P., Christen, M., Caviezel, A.: Stability of rigid body motion through an extended intermediate axis theorem: application to rockfall simulation. Multibody Sys. Dyn. **52**, 08 (2021)
11. Mangoni, D., Tasora, A., Peng, C.: Complex eigenvalue analysis of multibody problems via sparsity-preserving Krylov-schur iterations. Machines **11**(2), 218 (2023)
12. Minaker, B.P.: The tangent stiffness matrix in rigid multibody vehicle dynamics. Math. Comput. Model. Dyn. Syst. **21**(3), 288–310 (2014)
13. Peng, C., Tasora, A., Pin, L.: A method for the analysis of the aeroelastic stability of slender wind turbines and its validation (2023)
14. Przemieniecki, J.S.: Theory of Matrix Structural Analysis. Dover, Dover Civil and Mechanical Engineering (1985)

15. Shabana, A.A.: Dynamics of Multibody Systems. Cambridge University Press, Cambridge, England, fourth edition (2013)
16. Skjoldan, P., Hansen, M.: On the similarity of the Coleman and Lyapunov-Floquet transformation for modal analysis of blade rotor structures. J. Sound Vibr. **327**, 424–439 (2009)
17. Skjoldan, P.,Hansen, M.: Implicit Floquet analysis of wind turbines using tangent matrices of a nonlinear aeroelastic code. Wind Energy, **15**,275–287 (2012)
18. Tasora, A., et al.: Chrono: an open source multi-physics dynamics engine. In: Kozubek, T., Blaheta, R., Šístek, J., Rozložník, M., Čermák, M. (eds.) HPCSE 2015. LNCS, vol. 9611, pp. 19–49. Springer, Cham (2016). https://doi.org/10.1007/978-3-319-40361-8_2
19. Tasora, A., Masarati, P.: Analysis of rotating systems using general-purpose multibody dynamics. In: Pennacchi, P. (ed.) Proceedings of the 9th IFToMM International Conference on Rotor Dynamics. MMS, vol. 21, pp. 1689–1701. Springer, Cham (2015). https://doi.org/10.1007/978-3-319-06590-8_139
20. Thomas, O., Sénéchal, A., Deü, J.-F.: Hardening/softening behavior and reduced order modeling of nonlinear vibrations of rotating cantilever beams. Nonlinear Dyn. **86**, 1293–1318 (2016)
21. Zhao, G., Du, J., Wu, Z.: A geometric softening phenomenon of a rotating cantilever beam. Arch. Appl. Mech. **87**, 1049–1059 (2017)